Catalysis Today xxx (2016) xxx–xxx

Contents lists available at ScienceDirect

Catalysis Today

journal homepage: www.elsevier.com/locate/cattod

Pd-Ce nanoparticles supported on functional Fe-MIL-101-NH_2: An efficient catalyst for selective glycerol oxidation

Xinhang Li [a,b], Adrian Kaizen Tjiptoputro [a,b], Jun Ding [a], Jun Min Xue [a], Yinghuai Zhu [b,*]

[a] Department of Materials Sciences & Engineering, National University of Singapore, Engineering Drive 1, 117575, Singapore
[b] Institute of Chemical and Engineering Sciences, 1 Pesek Road, Jurong Island, 627833, Singapore

ARTICLE INFO

Article history:
Received 13 December 2015
Received in revised form 2 March 2016
Accepted 4 March 2016
Available online xxx

Keywords:
Metal organic frameworks
Nanocatalyst
Biomass conversion
Selective oxidation

ABSTRACT

Metal organic framework Fe-MIL-101-NH_2 was prepared at different reaction time. The morphology of the Fe-MIL-101-NH_2 slightly changed following a longer reaction time; the crystal structure remained. Neocuproine ligand coordinating palladium complex has demonstrated high activity in selective glycerol oxidation towards 1,3-dihydroxyacetone (DHA). Neocuproine ligand was attached to MOF Fe-MIL-101-NH_2 by forming an amide (CO—NH) bond in this work. The functional Fe-MIL-101-NH_2 was used as catalyst supports to hold palladium and cerium nanoparticles. The resulting composite of the Pd-Ce/Fe-MIL-101—N=$CH_{Neocuproine}$ was found to be a high efficient catalyst in the selective oxidation conversion of glycerol to dihydroxyacetone in comparison with catalysts Pd/Fe-MIL-101—N=$CH_{Neocuproine}$ and Pt-Bi/C. The catalysts and products were analyzed by FT-IR, XRD, SEM, TEM and ^{1}H, ^{13}C NMR spectroscopy. In addition, the supported catalyst is recyclable with sustainable activity.

1. Introduction

Glycerol is a by-product of biodiesel, which is produced from the transesterification reactions of oils and fats to their alkyl (methyl, ethyl, or propyl) esters [1]. Due to the increased demand of biodisel, glycerol production is continually increased and caused a major surplus [2–4]. Therefore, great research efforts have been added to discover either new applications or transformations towards high value-added chemicals using glycerol as a renewable resource via the reactions of the esterification [5], etherification [6], etc. Within all the potentially promising technologies, selective oxidations of glycerol into more value added chemicals are of great interest in current biomass research [7,8]. It has been reported that glycerol oxidation leads to the formation of a range of possible products, such as dihydroxyacetone, glyoxalic acid, and glyceric acid [9–15]. Dihydroxyacetone (DHA), a simple oxidation product of glycerol, is currently the most popularly used sunless tanners, which is the only active ingredient approved by the US Food and Drug Administration (FDA) for sunless tanning [16]. Currently, DHA is mainly produced from an atom-inefficient fermentation process [16]. Developments of new catalytic methods to produce DHA more efficiently are highly expected in the view of both industry and academia.

In catalysis, it has been well recognized that transition-metal nanoparticles (NPs) with a size range of around 5 nm or less own a higher ratio of the surface-to-volume. And thus enhance the interaction between catalytic active centers and reactants, enable more reactions to occur at the same time. The particles demonstrate unique physical and chemical properties, which are significantly different from their bulk counterparts. In addition, the NPs-based catalysts have the advantages of both homogeneous and heterogeneous classes such as well dispersion in reaction mixture and easily separation from product mixtures [17–20]. It has been well explored for catalytic oxidation of glycerol to use supported transition metal nanoparticles-based heterogeneous catalysts. The product distribution is highly depended upon both the catalysts and operation conditions. Catalyst Pt-Bi/C was investigated for the direct conversion of glycerol towards DHA, and demonstrated to be one of the most efficient catalysts [21]. A yield of 48.1% of DHA was achieved with the catalyst [21], and that is higher than catalysts of Pd-Ag NPs/C and Au NPs/C NPs which gave the yields of 44% and 40.7%, respectively [22,23].

On the other hand, carbon and zeolite have been widely used as catalyst supports to hold metal particles to drive chemical reactions. However, they both show inherent drawbacks. For zeolite support, only limited scope, less than 200 zeolites, are available. The pore sizes of zeolites are usually less than one nm; therefore it remains a big challenge to use zeolite in organic reactions in which larger molecules are involved [24]. For the carbon-related supports,

* Corresponding author.
E-mail address: zhu_yinghuai@ices.a-star.edu.sg (Y. Zhu).

http://dx.doi.org/10.1016/j.cattod.2016.03.044
0920-5861/

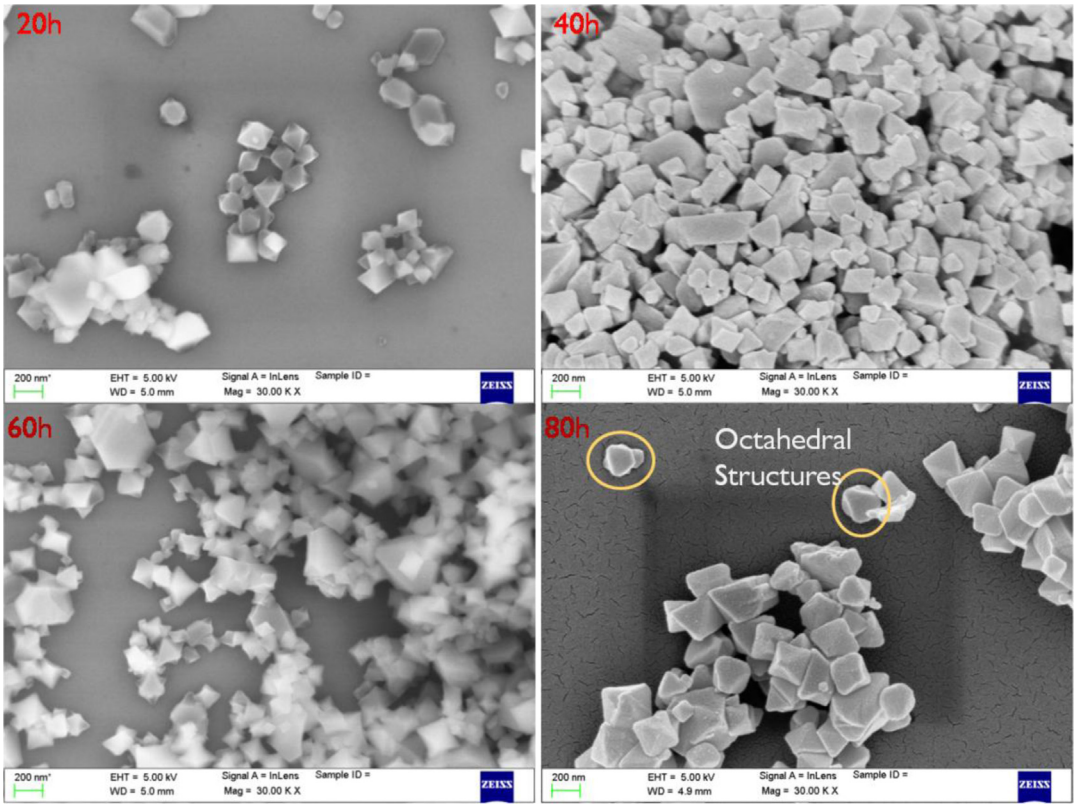

Fig. 1. SEM images of Fe-MIL-101-NH_2 at 30000× magnification with different reaction times. 20 h (upper left), 40 h (upper right), 60 h (lower left), and 80 h (lower right).

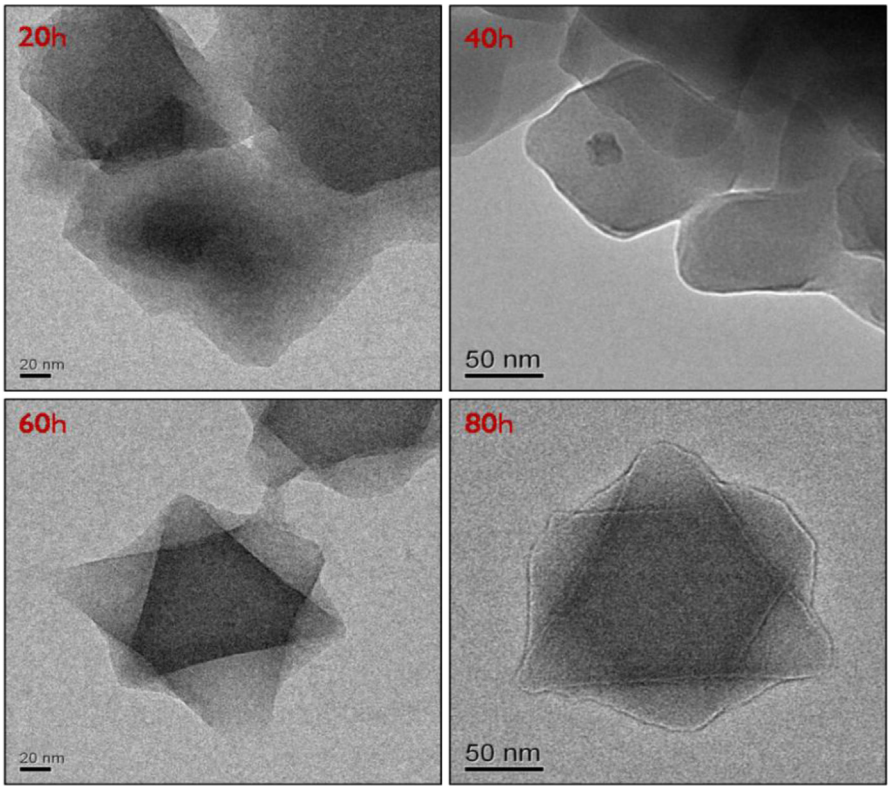

2.1

Fig. 2. TEM images of FE-MIL-101-NH_2 at 50000× magnification with different reaction times. 20 h (upper left), 40 h (upper right), 60 h (lower left), and 80 h (lower right).

the commercially available conventional mesoporous carbon supports tend to cause mass transport limitations of the reactants and carbon corrosion [25]. On the other hand, metal-organic framework (MOF) is a new emerging material consisting of metal ions and

Please cite this article in press as: X. Li, et al., Pd-Ce nanoparticles supported on functional Fe-MIL-101-NH_2: An efficient catalyst for selective glycerol oxidation, Catal. Today (2016), http://dx.doi.org/10.1016/j.cattod.2016.03.044

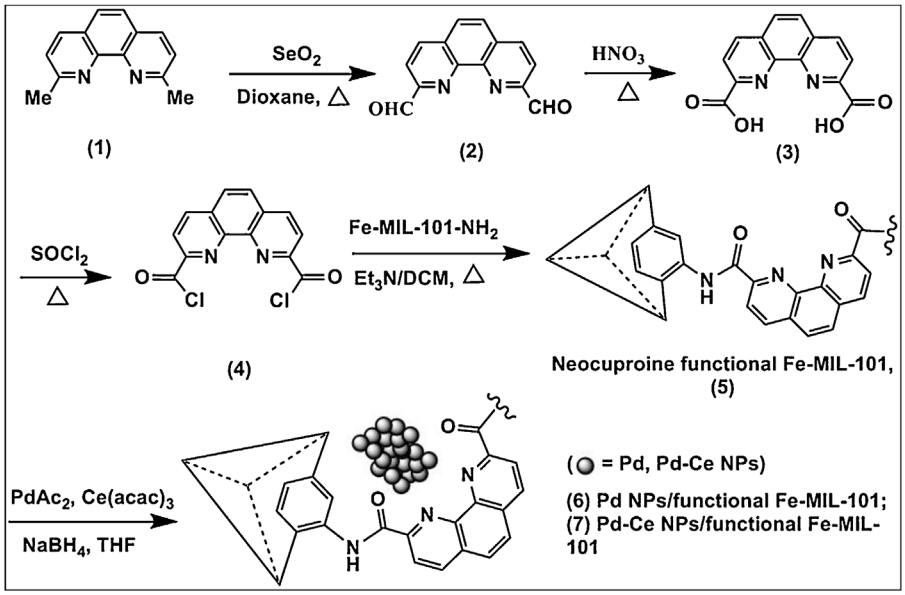

Scheme 1. Synthesis of functionalized Fe-MIL-101-NH_2 supported Pd-Ce nanoparticles.

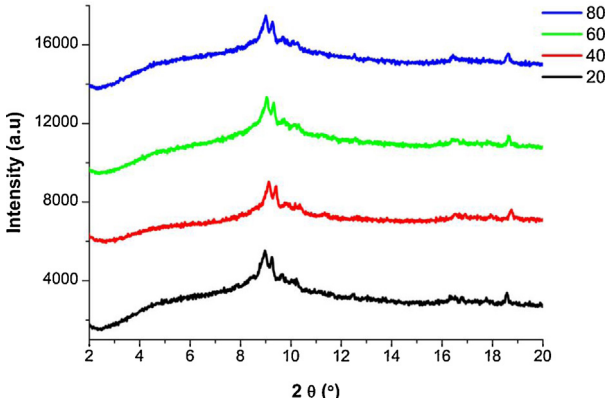

Fig. 3. XRD pattern comparison of Fe-MIL-101-NH_2 with different synthesis times.

coordinated organic ligands to form an ordered three-dimensional structure [26,27]. MOFs can be conveniently modified by changing the organic linkers or the metal ions. In addition, functional groups can also be easily attached onto the functional linkers to provide active sites. The flexibility provides MOFs unlimited structural possibilities, and that is crucial to craft MOFs for the required purposes [26,27]. Their unique properties such as exceptionally high surface areas, diversity in metals and coordinating ligands, tunable pore sizes, highly thermal stability (>400 °C) and strong base-resistance make them much more attractive as catalyst supports in comparison with traditionally used solids [26,27]. It is highly expected that MOFs could offer a promising industrial future. We have been studdying the potential applications of the metal organic frameworks supported metal nanoparticles-based catalysts for the oxidation of biomass-based glycerol to DHA. Fe-MIL-101-NH_2 was selected as support to hold metal nanoparticles-based catalysts due to its relatively long-term stability in air as well as high porosity [28,29]. Importantly, in the molecular structure of Fe-MIL-101-NH_2, there is amino (-NH_2) group at the *ortho-* site of the terephthalic acid linker [29]. The amino group enables further modification of the Fe-MIL-101-NH_2 to improve its functions without disrupting the carboxylate ligand that coordinates with the Fe ion. Herein, we report the synthetic methods and performances of the functional Fe-MIL-101-NH_2 supported catalysts for the selective oxidations of alcohols towards corresponding aldehydes and ketones.

2. Experimental

2.1. General

Dichloromethane (DCM) and acetonitrile were purchased from J.T Baker. Iron(III) Chloride hexahydrate, 2-aminoterephthalic acid, neocuproine, palladium acetate ($PdAc_2$), cerium(III) acetylacetonate ($Ce(acac)_3$), dimethylformamide (DMF), hexane, sodium borohydride, glycerol and other chemicals were purchased from Sigma-Aldrich. Water used in this work refers to de-ionic water. MOF Fe-MIL-101-NH_2 was prepared according to literature with slight modification [29]. The intermediates neocuproine dialdehydes [30,31], 2,9-dicarboxylic acid-1,10-phenanthroline [32] and 1,10-phenanthroline-2,9-dicarbonyl dichloride [33–35] were synthesized according to the previously reported methods.

2.2. Analysis methods

Nuclear magnetic resonance (NMR) spectra, ^1H and ^{13}C NMR, were recorded on a Bruker Fourier-Transform multinuclear NMR spectrometer at 400 and 100.6 MHz, relative to internal Me_4Si (TMS) standards. Fourier transform infrared spectroscopy (FT-IR) spectra were measured using a BIO-RAD spectrophotometer with the KBr self-support pellet technique and presented in the sequence of signal strength as strong (s), medium (m) and weak (w), and peak pattern as single (s), multiple (m) and broad (br). Raman spectroscopy was analyzed by a LabRam Raman spectrophotometer. Transmission electron microscopy (TEM) measurements were carried out on a JEOL Tecnai-G^2, FEI analyzer at 200 Kv. The Scanning Electron Microscopy (SEM) images were obtained using Zeiss Supra 40 FE SEM from Carl Zeiss AG (EHT = 5.0 kV). Using the same SEM setup, elemental analysis data are obtained by Point & ID method using X-Max Silicon Drift Detector (SDD) 50mm2 from Oxford Instruments. Inductively coupled plasma (ICP) analysis was determined using a VISTA-MPX, CCD Simultaneous ICP-OES analyzer. X-Ray photoelectron spectrometer (XPS) was performed with an ESCALAB 250 analyzer.

Please cite this article in press as: X. Li, et al., Pd-Ce nanoparticles supported on functional Fe-MIL-101-NH_2: An efficient catalyst for selective glycerol oxidation, Catal. Today (2016), http://dx.doi.org/10.1016/j.cattod.2016.03.044

2.3. Synthesis of neocuproine-based functional ligands

Neocuproine dialdehydes, 2,9-dicarboxylic acid-1,10-phenanthroline and 1,10-phenanthroline-2,9-dicarbonyl dichloride were synthesized according to literature [30–35]. All the products were characterized by ^{1}H, ^{13}C NMR spectra and confirmed by comparing with previous reports.

Neocuproine dialdehydes, $C_{14}H_8N_2O_2$, yield 60%. ^{1}H NMR (DMSO-d_6, ppm), δ = 10.37 (s, 2H, 2CHO), 8.78 (d, 2H, $C_{12}H_2N_2$), 8.28 (d, 2H, $C_{12}H_2N_2$), 8.27 (d, 2H, $C_{12}H_2N_2$). ^{13}C NMR (DMSO-d_6, ppm), δ = 193.68 (CHO), 152.12, 145.19, 138.38, 131.39, 129.19, 120.07 ($C_{12}H_6N_2$). Literature results [32]: ^{1}H NMR (DMSO-d_6, ppm), δ = 10.34 (s, 2H), 8.77 (d, 2H), 8.28 (d, 2H), 8.27 (d, 2H). ^{13}C NMR (DMSO-d_6, ppm), δ = 194.1, 152.6, 145.7, 138.9, 131.9, 129.7, 120.6.

2,9-Dicarboxylic acid-1,10-phenanthroline, $C_{14}H_8N_2O_4$, yield 71%. ^{1}H NMR (DMSO-d_6, ppm), δ = 8.74 (d, 2H, $C_{12}H_2N_2$), 8.42 (d, 2H, $C_{12}H_2N_2$), 8.20 (d, 2H, $C_{12}H_2N_2$). ^{13}C NMR (DMSO-d_6, ppm), δ = 166.19, (CO_2H), 148.22, 144.66, 138.14, 130.44, 128.36, 123.41 ($C_{12}H_6N_2$). Literature results [32]: ^{1}H NMR (DMSO-d_6, ppm), δ = 8.74 (d, 2H), 8.42 (d, 2H), 8.22 (d, 2H). ^{13}C NMR (DMSO-d_6, ppm), δ = 166.7, 148.6, 145.1, 138.7, 130.9, 128.8, 124.3.

1,10-Phenanthroline-2,9-dicarbonyl dichloride, $C_{14}H_6Cl_2N_2O_2$, was prepared by the reaction of 2,9-dicarboxylic acid-1,10-phenanthroline and $SOCl_2$ followed by remove of excess $SOCl_2$ in vacuum [33–35]. The resulting was dissolved with anhydrous dichloromethane for next steps without further purification and characterization.

2.4. Synthesis of MOF Fe-MIL-101

Fe-MIL-101-NH2 was synthesized according to the previously published protocols with slight modification of further washing with DCM and hexane [29]. In brief, 450.0 mg (2.5 mmol) of 2-aminoterephthalic acid (NH_2—H_2BDC) in 15.0 mL of DMF with a solution of 1350.0 mg (5.0 mmol) of FeCl3·6H2O in 15.0 mL of DMF is mixed and stirred thoroughly. The mixture is then treated in a stainless steel autoclave for 20 h at 110 °C. The resultant dark brown solid is then recovered by centrifuge, filtered and washed with DMF and subsequently DCM to remove un-reacted ligands. Hexane is also used to wash to assist with the drying process, after which the sample is dried at ambient conditions. After drying, dark brown solid as a product is obtained. The procedure is then repeated with modification to the reaction time in the autoclave, namely at 40, 60 and 80 h.

2.5. Synthesis of neocuproine functionalized Fe-MIL-101

A 100.0 mg of Fe-MIL-101-NH_2 was mixed in about 10.0 mL of anhydrous dichloromethane. A solution of 1,10-phenanthroline-2,9-dicarbonyl dichloride by mixing 300.0 mg *in situ* prepared 1,10-phenanthroline-2,9-dicarbonyl dichloride in 15.0 mL of DCM as described in part 2.3. The dichloride solution was next added drop-wise into the Fe-MIL-101-NH_2/DCM mixture at room temperature followed by addition of 0.5 mL of Et_3N. The mixture was then heated to reflux with continuous stirring for 18 h. The neocuproine functionalized Fe-MIL-101-NH_2 was collected by centrifugation and washed with DCM (3 × 10.0 mL) dried in a vacuum to give 100.0 mg red-brown solid product. The product was subjected to characterize by XRD and FT-IR.

2.6. Synthesis of metal nanoparticles supported functionalized Fe-MIL-101-NH_2

After synthesizing the neocuproine functionalized Fe-MIL-101-NH_2, we used the compound to support palladium and palladium-cerium nanoparticles. The supporting of metal nanoparticles on Fe-MIL-101-NH_2 was carried out by using transition metal complex precursors $PdAc_2$ (11.4 mg) and $Ce(acac)_3$ (17.5 mg) dissolved in tetrahydrofuran (THF) (30.0 mL). A 200.0 mg of Fe-MIL-101-NH_2 was added to above solution, and the resulting mixture was stirred for one hour. The mixture was then cooled to 0 °C by immersing the flask in ice. After which, 3.0 mL of $NaBH_4$ solutions were added drop-wise into the mixture. The final product was obtained by centrifuge, washed with methanol (3 × 10.0 mL) and diethyl ether (2 × 10.0 mL) in sequence followed by dried in vacuum to obtain 195.0 mg gray powder product. The prod-

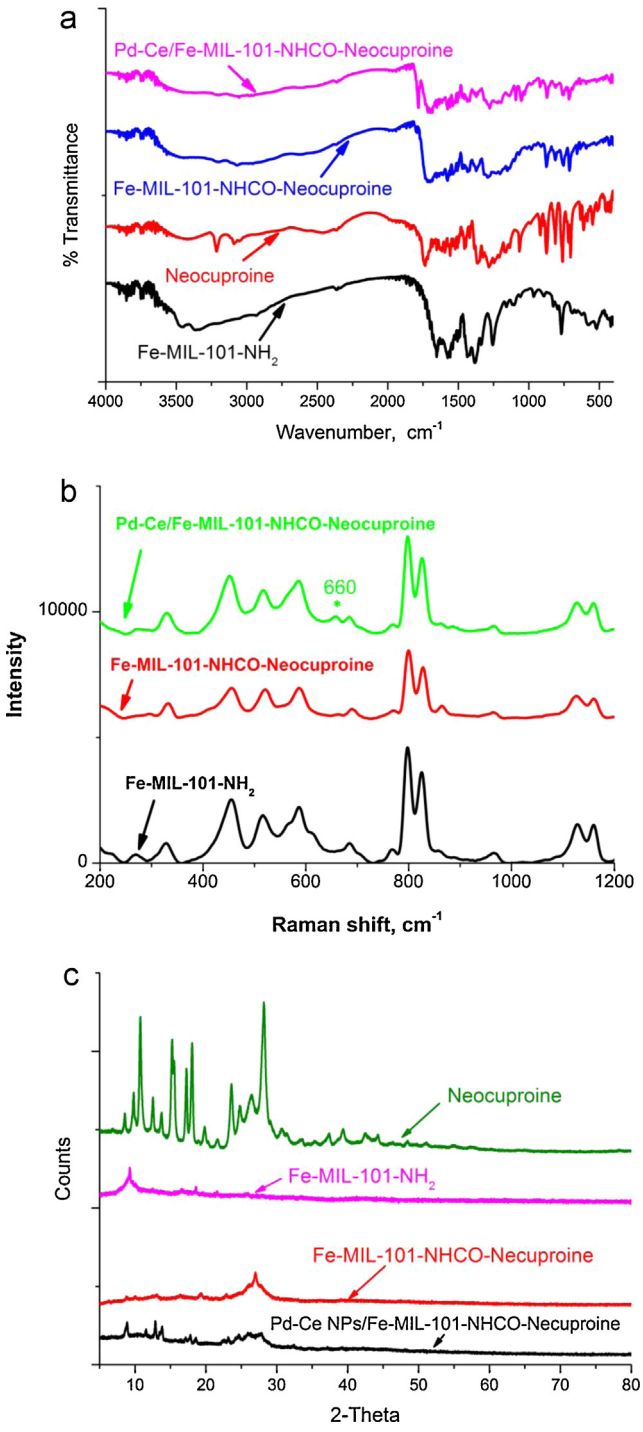

Fig. 4. FT-IR (a), Raman (b) and XRD spectra of the support of functionalized Fe-MIL-101-NH_2 and catalyst Pd-Ce NPs/functionalized Fe-MIL-101-NH_2.

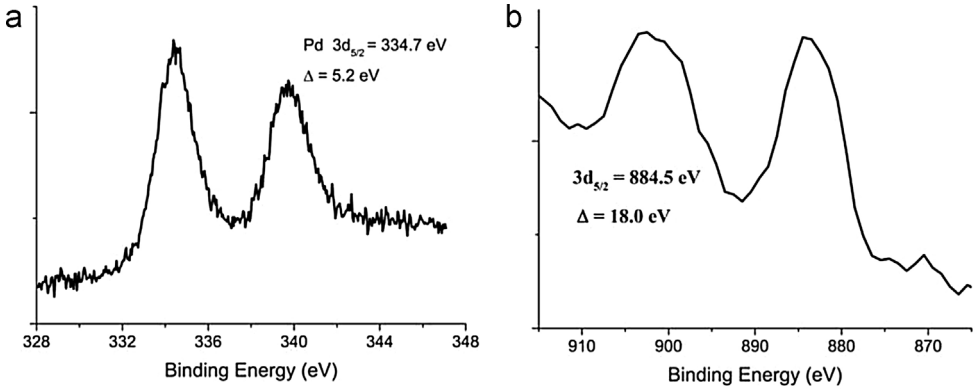

Fig. 5. XPS of catalyst Pd-Ce NPs/functionalized Fe-MIL-101-NH_2.

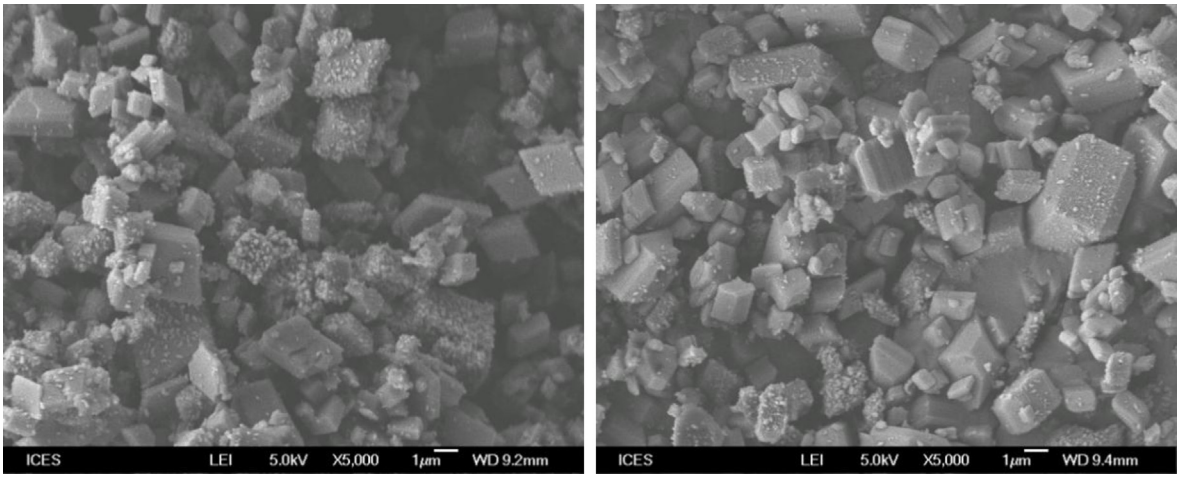

Fig. 6. SEM images of pristine (left) and functionalized (right) Fe-MIL-101-NH_2 at 5000× magnification.

ucts were subjected to analysis by TEM, SEM, XRD and FT-IR. The same procedure is used to prepare catalysts Pd/functional Fe-MIL-101-NH_2, Au/functional Fe-MIL-101-NH_2 and Ce/functional Fe-MIL-101-NH_2.

2.7. General procedure for glycerol oxidation to DHA

A 70.0 mL solution of acetonitrile/water (6:1, v/v) was used to dissolve glycerol (1610.0 mg, 17.5 mmol). A 7.0 mL of this glycerol solution was next mixed with 25.0 mg of each catalyst in a batch reactor. A magnetic stirring bar was also placed inside each one of the batch reactor. The containers were then placed in a pressure chamber, and the setup was flushed with oxygen. A reaction condition of 60 °C and pressure at 20 psi was maintained for 6 h. After reaction, the reactor was cooled to room temperature and the vessels were taken out for filtration. The mixtures were filtered through syringe filters to remove the solid catalysts. The filtrates were collected in separate round bottom flasks. The solvent was removed under reduced pressure by using a rotary evaporator, and the resulting product mixtures were analyzed using gas chromatography (Agilent Gas Chromatograph (GC-FID) 6850, column: Agilent 19091Z-433, flow rate: 1.6 mL/min) and the high-performance liquid chromatography (Agilent, column: Aminex HPX-87H Column, wash solution: 0.02 N H_2SO_4, flow rate 1.0 mL/min, column temperature 60 °C, UV detector 210 nm). The yield was calculated according to the amount of glycerol added. In addition, the products were analyzed and identified by ^1H and ^{13}C NMR.

Dihydroxyacetone, $HOCH_2C(=O)CH_2OH$, yield 55% (with dimer). ^1H NMR (D_2O, ppm), δ = 4.29 (s, 4H, 2C$\underline{H}_2$). ^{13}C NMR (D_2O, ppm), δ = 211.93 (C$\underline{O}$), 64.77 (-$\underline{C}H_2$-).

Pentane-1,5-dial, $HC(=O)(CH_2)_3CHO$, yield 69% (with dimer). ^1H NMR (DMSO-d_6, ppm), δ = 9.627 (s, 2H, 2C$\underline{H}$O), 2.460 (t, 4H, 2C(=O)-$\underline{C}H_2$), 1.76-1.58 (m, 2H, $\underline{C}H_2$). ^{13}C NMR (D_2O, ppm), δ = 203.45 (C$\underline{O}$), 42.04 (CO-$\underline{C}H_2$-), 14.08 (-$\underline{C}H_2$-).

Benzaldehyde, PhCHO, yield 56%. ^1H NMR ($CDCl_3$, ppm), δ = 10.01 (s, H, C$\underline{H}$O), 8.13-7.27 (m, 5H, $C_6\underline{H}_5$). ^{13}C NMR ($CDCl_3$, ppm), δ = 192.41 (C$\underline{H}$O), 136.38, 134.46, 129.73, 129.52 ($\underline{C}_6H_5$).

3. Results and discussion

MOF Fe-MIL-101-NH_2 was prepared according to literature with slight modification [29]. The operation was carried out at a different time to investigate the effect of reaction time on the morphology and structure of the MOF. The SEM (Fig. 1) and TEM images (Fig. 2) shown below illustrate a change in the morphology of Fe-MIL-101-NH_2 as the reaction time is increased. It suggests that as reaction time is increased, the incidence of octagonal structure increases as compared to the tetragonal structure encountered using the standard reaction time (20 h). However, there is no obvious increase in the single-crystal size as reaction time is prolonged.

Fig. 3 shows the XRD spectra of MOF Fe-MIL-101-NH_2 prepared at the different time points. It can be seen that the peak's shape and position of the XRD is similar across all reaction times. The results suggest that the crystalline Fe-MIL-101-NH_2 structure is still there after extending reaction time to 40 h, 60 h and 80 h, respectively. As there is no obvious change in the crystal structure and only mor-

Please cite this article in press as: X. Li, et al., Pd-Ce nanoparticles supported on functional Fe-MIL-101-NH_2: An efficient catalyst for selective glycerol oxidation, Catal. Today (2016), http://dx.doi.org/10.1016/j.cattod.2016.03.044

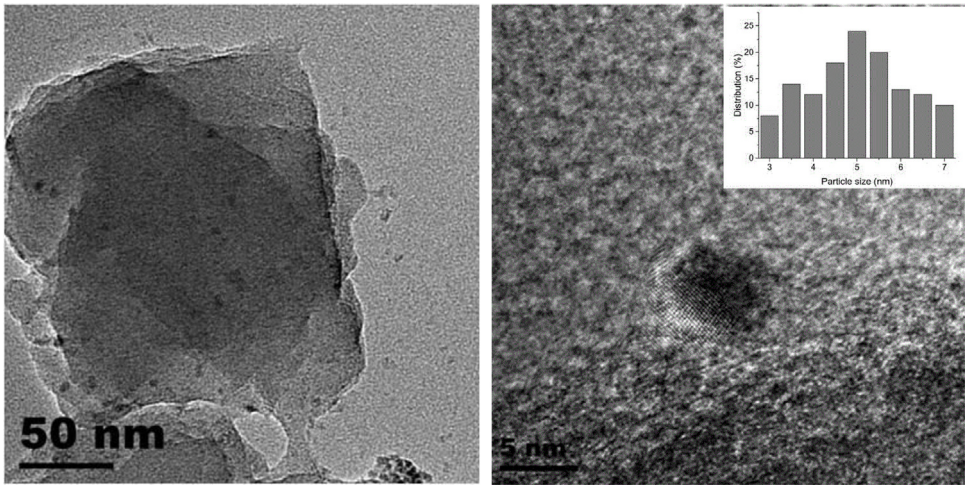

Fig. 7. TEM images and particle size histogram of the catalyst composit Pd-Ce NPs/functionalized Fe-MIL-101-NH_2.

phology seems to be changed in the modification of the reaction time in synthesizing Fe-MIL-101-NH_2, the commonly used baseline of 20 h have been used for the synthesis of materials of the subsequent steps of this work.

It has been demonstrated that neocuproine coordinated palladium complex, $((\eta^2$-neocuproine)$PdOAc)_2(OTf)_2$, to be the most active homogeneous catalyst in glycerol selective oxidation towards DHA [36]. The neocuproine ligand plays a crucial role in the catalytic procedure to control the stereo effects [36]. Therefore, in the work, neocuproine ligand has been attached onto Fe-MIL-101-NH_2 by forming an amide bond (CO—NH) and that further been used as support to hold the transition metal nanoparticles-based catalysts. Similar with other MOF supported metal nanoparticle-based catalysts such as Pt NPs/MIL-101 [37] and Pd NPs/MOF [38], transition metal nanoparticles used in this work could be immobilized inside the pores of the functional Fe-MIL-101-NH_2. During the functionalization of Fe-MIL-101-NH_2, as shown in Scheme 1, neocuproine (**1**) was first oxidized to dialdehyde (**2**) using selenium dioxide [30,31]. Intermediate (**2**) was subsequently oxidized with nitric acid to form 1,10-phenanthroline-2,9-dicarboxylic acid (**3**) [32]. Products **2** and **3** were characterized by ^1H, ^{13}C NMR spectra. The results are consistent with literature reports [32]. The latter compound was *in situ* converted into 1,10-phenanthroline-2,9-diacyl chloride **(4)** by reacting with thionyl chloride [32–35]. The obtained intermediate **(4)** was immediately reacted with Fe-MIL-101-NH_2 without being isolated to provide the neocuproine functionalized MOFs **(5)**. Transition metal nanoparticles (NPs)-based catalysts such as palladium NPs and palladium-cerium NPs were immobilized on the supports by co-precipitation methods by reducing corresponding precursors $PdAc_2$ and $Ce(acac)_3$, respectively with sodium borohydride. The products were characterized by XRD, TEM, SEM, NMR, XPS and FT-IR.

The FT-IR, Raman and XRD spectroscopy were used to characterize support precursor Fe-MIL-101-NH_2, neocuproine ligand, functionalized Fe-MIL-101-NH_2, and catalyst Pd-Ce NPs/functionalized Fe-MIL-101-NH_2 as shown in Fig. 4. In FT-IR spectra, normal absorptions for functional groups were observed. The pristine Fe-MIL-101-NH_2, the broad absorptions at 3468 and 3367 cm^{-1} can be attributed to the N—H stretching vibrations. After functionalization with neocuproine ligand, the N—H stretching bands in the amide bonds down-shifted to 3210 and 3213 cm^{-1} (weak and broad) for functional Fe-MIL-101-NH_2 and Pd-Ce NPs/functional Fe-MIL-101-NH_2, respectively. Neocuproine ligand shows a strong absorption at 1736 cm^{-1} which can be attributed to the aromatic C=C stretching vibrations. After attaching to MOF, the peak shifted to 1717 and 1720 cm^{-1} for functional Fe-MIL-101-NH_2 and Pd-Ce NPs/functional Fe-MIL-101-NH_2, respectively.

In Raman spectra as shown in Fig. 4 **(b)**, a new peak at 660 cm^{-1} appeared for Pd-Ce NPs/functional Fe-MIL-101-NH_2 in comparison with absorptions of the pristine and functional Fe-MIL-101-NH_2. Since the Raman spectroscopy is not able to detect pure metallic phase [39]. However, Raman spectroscopy is able to detect the incorporation of small atoms such as O and C, into the lattice of these metallic phases. Furthermore, $NaBH_4$ is commonly used to reduce palladium complexes to generate Pd° particles. The resulting Pd° is not detectable in Raman. Therefore, the new peak is most probably contributed from vibration of the Ce—O bond in Ce_2O_3, which is produced from the reaction of $Ce(acac)_3$ in our system.

The oxidation states of the supported metal nanoparticles were identified by XPS analysis. As shown in Fig. 5(a), the Pd 3d showed peaks at 334.7 and 339.9 eV (Δ = 5.2 eV), which were consistent with Pd° [40]. Two peaks were detected for the Ce 3d (Fig. 5(b)), which appeared at the binding energy (902.5 and 884.5 eV) expected for Ce^{3+} species [41]. In XRD spectra, the functionalized Fe-MIL-101-NH_2 and catalyst Pd-Ce NPs/functionalized Fe-MIL-101-NH_2 show similar absorption patterns.

The functional products were also analyzed by SEM spectroscopy. As shown in Fig. 6, no significant differences were observed in SEM images for Fe-MIL-101-NH_2 and after modification with neocuproine ligand. All the above results confirm that the palladium and cerium-based nanocatalyst were supported on the functional MOF Fe-MIL-101-NH_2.

Fig. 7 shows the TEM images of the supported catalyst Pd-Ce NPs/functionalized Fe-MIL-101-NH_2. It can be seen that the Pd-Ce NPs are small, with an average particle size of ~5 nm (determined from the measurement of ~130 particles), and well dispersed on the support. The catalysts were also analyzed by ICP and SEM-EDX to identify metal loading amount and shown that the total metal is around 5 wt% according to ICP analysis. The catalyst was examined for alcohol oxidation reactions. A yield of 55% of DHA was obtained by the catalyst, and that is slightly higher than literature results [21–23]. For comparison, catalysts Pd NPs/functional Fe-MIL-101-NH_2, Ce NPs/functional Fe-MIL-101-NH_2 and Au NPs/functional Fe-MIL-101-NH_2 were prepared in the same method and examined for glycerol oxidation towards DHA. The DHA yields of 17%, 4% and 10% were obtained, respectively. Although the catalyst shows lower activity in comparison with corresponding homogeneous catalyst $((\eta^2$-neocuproine)$PdOAc)_2(OTf)_2$, which gives a high yield of 69% with the oxygen (1 atm) oxidant [36], it can be recovered conveniently either by filter or centrifugation. The catalyst

Please cite this article in press as: X. Li, et al., Pd-Ce nanoparticles supported on functional Fe-MIL-101-NH_2: An efficient catalyst for selective glycerol oxidation, Catal. Today (2016), http://dx.doi.org/10.1016/j.cattod.2016.03.044

has been recovered and reused at least three times with sustained activity. To investigate the leaching of Pd-Ce nanoparticles, the samples of the filtrate plus washings obtained from above standard reactions were subjected to ICP analysis that showed the concentrations of Pd and Ce was less than 2.7 and 3.5 ppm, respectively in each measurement. In addition, the standard reaction was conducted with recovered filtrate, but no product could be isolated. The results suggested that the supported Pd-Ce catalysts, rather than the leached metal species, provide the catalytic performance. However, same as other homogeneous catalyses, remove of complex $((\eta^2$-neocuproine)PdOAc$)_2(OTf)_2$ from the product mixture to meet the industrial standards remains a big challenge, and that could prevent its wide application of the technology, particularly in personal care products.

To investigate the substrate scope, oxidation of the ethanol, 1,5-pentanediol and benzyl alcohols were carried out under the same conditions in the presence of catalyst Pd-Ce NPs/functional Fe-MIL-101-NH_2. Product acetaldehyde, pentane-1,5-dial and benzaldehyde were obtained in the yields of 64% (GC-based), 49%, and 56%, respectively.

Based on the obtained results, the functional Fe-MIL-101-NH_2 supported catalysts showed an activity sequence of Pd-Ce > Pd > Au > Ce under same conditions for the glycerol selective oxidation towards DHA. Although the real mechanism is not clear yet at this stage, the Ce^{3+} species could be crucial to improve the Pd based catalyst in this system either to activate Pd active center or the substrate. The mechanism investigation is undergoing.

4. Conclusions

In this work, metal organic framework Fe-MIL-101-NH_2 was synthesized in varying reaction time. It was found that the morphology of Fe-MIL-101-NH_2 slightly changed following a longer reaction time; the crystal structure remained. The MOF was functionalized with neocuproine ligand and further used as supports to prepare catalysts of M NPs/Fe-MIL-101—N=$CH_{Neocuproine}$ (M = Pd, Pd-Ce, Ce and Au). Catalyst Pd-Ce/Fe-MIL-101—N=$CH_{Neocuproine}$ showed good activity for selective oxidation of glycerol and other alcohols to produce corresponding aldehydes. Considering the good activity and recyclability of the catalyst, we expect our prototype catalyst to find broader applications in both academia and fine chemical industry, particularly in the area of biomass conversion towards high value-added products such as DHA.

Acknowledgements

We thank SMART *(Singapore-MIT Alliance for Research and Technology)* Innovation grant and ICES, A*STAR for financial support. Thanks Ms Wan Zhang to help analyze XPS and Ms Cheng Shuying to analyze Raman.

References

[1] B. Gutsche, Fett/Lipid 99 (1997) 418–427.
[2] R. Christoph, B. Schmidt, U. Steinberner, W. Dilla, Glycerol, in Ullmann's Encyclopedia of Industrial Chemistry, Wiley-VCH Verlag GmbH & Co. KGaA, 2000.
[3] J.-M. Clacens, Y. Pouilloux, J. Barrault, J. Appl. Catal. A: Gen. 227 (2002) 181–190.
[4] S.S. Yazadani, R. Gonzalez, Curr. Opin. Biotechnol. 18 (2007) 213–219.
[5] M.A. Betiha, Hassan M.A. Hassan, E.A. El-Sharkawy, A.M. Al-Sabagh, M.F. Menoufy, H.-E.M. Abdelmoniem, Appl. Catal. B Env. 182 (2016) 15–25.
[6] H.J. Leea, D. Seunga, K.S. Junga, H. Kimb, I.N. Filimonova, Appl. Catal. A Gen. 390 (2010) 235–244.
[7] M. Pagliaro, R. Ciriminna, H. Kimura, M. Rossi, P.C. Della, Angew. Chem. Int. Ed. Engl. 46 (2007) 4434–4440.
[8] B. Katryniok, H. Kimura, E. Skrzyńska, J.-S. Girardon, P. Fongarland, M. Capron, R. Ducoulombier, N. Mimura, S. Paul, F. Dumeignil, Green Chem. 13 (2011) 1960–1979.
[9] H. Kimura, K. Tsuto, T. Wakisaka, Y. Kazumi, Y. Inaya, Appl. Catal. A: Gen. 96 (1993) 217–228.
[10] T. Mallat, A. Baiker, Catal. Today 24 (1995) 143–150.
[11] P. Fordham, M. Besson, P. Gallezot, Appl. Catal. A: Gen. 133 (1995) 179–184.
[12] S. Carrettin, P. McMorn, P. Johnston, K. Griffin, C.J. Kiely, G. Hutchings, J. Phys. Chem. Chem. Phys. 5 (2003) 1329–1336.
[13] S. Carrettin, P. McMorn, P. Johnston, K. Griffin, C.J. Kiely, G. Hutchings, Chem. Commun. (2002) 696–697.
[14] E.G. Rodrigues, M.F.R. Pereira, J.J. Delgado, X. Chen, J.J.M. Órfão, Catal. Commun. 16 (2011) 64–69.
[15] D. Liang, J. Gao, H. Sun, P. Chen, Z. Hou, X. Zheng, Appl. Catal. B Env. 106 (2011) 423–432.
[16] Dihydroxyacetone, Market Research Report, 2012 http://marketpublishers.com.
[17] R. Ferrando, J. Jellinek, R.L. Johnston, Chem. Rev. 108 (2008) 845–910.
[18] Y. Zhu, C.N. Lee, R.A. Kemp, N.S. Hosmane, J.A. Maguire, Chem. Asian J. 3 (2008) 650–662.
[19] Y. Zhu, L.P. Stubbs, F. Ho, R. Liu, C.P. Ship, J.A. Maguire, N.S. Hosmane, ChemCatChem 2 (2010) 365–374.
[20] Y. Zhu, N.S. Hosmane, Coord. Chem. Rev. 293–294 (2015) 357–367.
[21] W. Hu, D. Knight, B. Lowry, A. Varma, Ind. Eng. Chem. Res. 49 (2010) 10876–10882.
[22] S. Hirasawa, Y. Nakagawa, K. Tomishige, Catal. Sci. Technol. 2 (2012) 1150–1152.
[23] C.A. Nunes, M.C. Guerreiro, J. Mol. Catal. A Chem. 370 (2013) 145–151.
[24] C.D. Chudasama, J. Sebastian, R.V. Jasra, Ind. Eng. Chem. Res. 44 (2005) 1780–1786.
[25] J.P. Meyers, R.M. Darling, J. Electrochem. Soc. 153 (2006) A1432–A1442.
[26] M. Meilikhov, K. Yusenko, D. Esken, S. Turner, G. Van Tendeloo, R.A. Fischer, Eur. J. Inorg. Chem. 49 (2010) 3701–3714.
[27] S.T. Meek, J.A. Greathouse, M.D. Allendorf, Adv. Mater. 23 (2011) 249–267.
[28] A. Henschel, K. Gedrich, R. Kraehnert, S. Kaskel, Chem. Commun. 35 (2008) 4192–4194.
[29] S. Bauer, C. Serre, T. Devic, P. Horcajada, J. Marrot, G. Ferey, N. Stock, Inorg. Chem. 47 (2008) 7568–7576.
[30] C.J. Chandler, L.W. Deady, J.A. Reiss, J. Heterocycl. Chem. 18 (1981) 599–601.
[31] S. Goswami, A.K. Adak, Synth. Commun. 33 (2003) 475–480.
[32] A. De Cian, E. De Lemos, J.-L. Mergny, M.P. Teulade-Fichou, D. Monchaud, J. Am. Chem. Soc. 129 (2007) 1856–1857.
[33] C.J. Chandler, L.W. Deady, J.A. Reiss, V. Tzimos, J. Heterocycl. Chem. 19 (1982) 1017–1019.
[34] M. Galletta, S. Scaravaggi, E. Macerata, A. Famulari, A. Mele, W. Panzeri, F. Sansone, A. Casnati, M. Mariani, Dalton Trans. 42 (2013) 16930–16938.
[35] C.-L. Xiao, C.-Z. Wang, L.-Y. Yuan, B. Li, H. He, S. Wang, Y.-L. Zhao, Z.-F. Chai, W.-Q. Shi, Inorg. Chem. 53 (2014) 1712–1720.
[36] R.M. Painter, D.M. Pearson, R.M. Waymouth, Angew. Chem. Int. Ed. 49 (2010) 9456–9459.
[37] A. Aijaz, A. Karkamkar, Y.J. Choi, N. Tsumori, E. Rönnebro, T. Autrey, H. Shioyama, Q. Xu, J. Am. Chem. Soc. 134 (2012) 13926–13929.
[38] A. Aijaz, Q.L. Zhu, N. Tsumori, T. Akita, Q. Xu, Chem. Commun. 51 (2015) 2577–2580.
[39] W.H. Weber, Raman Scattering in Materials Science, in: W.H. Weber, R. Merlin (Eds.), Springer-Verlag, New York, 2000.
[40] J.F. Moulder, W.F. Stickle, P.E. Sobol, K.D. Bomben, Handbook of X-ray Photoelectron Spectroscopy, Physical Electronics Inc., USA, 1995, pp. 118–119.
[41] J.F. Moulder, W.F. Stickle, P.E. Sobol, K.D. Bomben, Handbook of X-ray Photoelectron Spectroscopy, Physical Electronics Inc., USA, 1995, pp. 142–143.

Please cite this article in press as: X. Li, et al., Pd-Ce nanoparticles supported on functional Fe-MIL-101-NH_2: An efficient catalyst for selective glycerol oxidation, Catal. Today (2016), http://dx.doi.org/10.1016/j.cattod.2016.03.044